Patient Specific Hardware-in-the-Loop Testing of Cerebrospinal Fluid Shunt Systems

Gehlen, Manuel ; Kurtcuoglu, Vartan ; Schmid Daners, Marianne

Abstract: GOAL The development of increasingly sophisticated cerebrospinal fluid (CSF) shunts calls for test beds that can reproduce an ever larger range of physiologic and pathophysiologic behaviors. In particular, upcoming smart and active devices will require extensive testing under complex dynamic conditions. Herein, we describe a test bed that allows for fast, cost effective, and realistic in vitro testing of active and passive, gravitational and nongravitational CSF shunts based on the hardware-in-the-loop principle. METHODS The shunt to be tested is placed in a dynamic in vitro setup that interfaces with a mathematical model of the patient's relevant physiology, which is evaluated numerically in real time. The model parameters can be identified using standard clinical tests. The test bed accounts for posture-dependent behavior and viscoelastic effects. RESULTS Simulations of infusion tests, of intracranial pressure modulation by cardiovascular action, and of the effects of postural changes show good agreement with published results. Evaluation of valves without and with gravitational units show in modeled sitting patients the expected behavior of overdrainage and avoidance thereof, respectively. Finally, a 24-h test cycle based on recorded patient data elucidates the interaction between patient and shunt system expressed by drainage rate and intracranial pressure during typical daily activities. CONCLUSION We envision this test bed as a tool to quantify a shunt's performance within a realistic yet reproducible testing environment. SIGNIFICANCE The test bed can improve our understanding of the complex interaction between patient and shunt system and may catalyze the development of active shunts, while reducing the number of necessary in vivo experiments.

DOI: https://doi.org/10.1109/TBME.2015.2457681

Patient Specific Hardware-in-the-Loop Testing of Cerebrospinal Fluid Shunt Systems

Manuel Gehlen, Vartan Kurtcuoglu, and Marianne Schmid Daners

***Abstract*—*Goal:* The development of increasingly sophisticated cerebrospinal fluid (CSF) shunts calls for test beds that can reproduce an ever larger range of physiologic and pathophysiologic behaviors. In particular, upcoming smart and active devices will require extensive testing under complex dynamic conditions. Herein, we describe a test bed that allows for fast, cost-effective and realistic *in vitro* testing of active and passive, gravitational and non-gravitational CSF shunts based on the hardware-in-the-loop principle. *Methods:* The shunt to be tested is placed in a dynamic *in vitro* setup that interfaces with a mathematical model of the patient's relevant physiology, which is evaluated numerically in real-time. The model parameters can be identified using standard clinical tests. The test bed accounts for posture dependent behavior and viscoelastic effects. *Results:* Simulations of infusion tests, of intracranial pressure modulation by cardiovascular action, and of the effects of postural changes show good agreement with published results. Evaluation of valves without and with gravitational units show in modeled sitting patients the expected behavior of overdrainage and avoidance thereof, respectively. Finally, a 24-hour test cycle based on recorded patient data elucidates the interaction between patient and shunt system expressed by drainage rate and intracranial pressure during typical daily activities. *Conclusion:* We envision this test bed as a tool to quantify a shunt's performance within a realistic yet reproducible testing environment. *Significance:* The test bed can improve our understanding of the complex interaction between patient and shunt system and may catalyze the development of active shunts, while reducing the number of necessary *in vivo* experiments.**

***Index Terms*—hardware-in-the-loop, in vitro, testing, hydrocephalus, CSF, shunt, posture, animal testing alternatives.**

I. Introduction

In our current, evolving understanding, "hydrocephalus is an active distension of the ventricular system of the brain related to inadequate passage of CSF from its point of production within the ventricular system to its point of absorption into the systemic circulation" [1]. While this distension leads to elevated intracranial pressure (ICP) and a deformation of the brain parenchyma in the short term, it can cause a degeneration of this tissue in the long term. The accompanying symptoms range from headaches to dementia, gait disturbance, and urinary incontinence [2]. Hydrocephalus is usually treated by diverting CSF from the cerebral ventricles through a shunt into the peritoneal space. Although implantable ventriculoperitoneal shunts have been used since the 1960s [3], the overall failure rate is still high (38% after 1 year and 48% after 2 years [4]). The most common modes of failure are over- or underdrainage, obstruction, and infection [5], [6].

To prevent siphoning-induced overdrainage in upright postures, shunt valves can be complemented by gravitational units, anti-siphon devices, and adjustable mechanisms [3], which lead to increasingly complex shunt systems. This unsatisfactory situation has led to the vision of an active and smart shunt that could overcome the drawbacks of current systems through continuous monitoring of the patient using integrated sensors and feedback controlled drainage [7].

For the existing passive shunts, a large number of *in vitro* studies has already been performed to analyze their fluid dynamic properties, the effect of ICP pulsations and posture on these properties, and long-term stability [8]–[14]. In these studies, the intracranial and peritoneal pressures were assumed to be independent of CSF drainage. Yet in reality, drainage does decrease mean ICP, in general also ventricular volume, and may in addition influence the amplitude of ICP pulsations [15], [16]. These effects have been demonstrated in other setups that replicated parts of the patient's CSF system *in vitro* [17]–[21].

For the envisioned active valves, this interdependence of valve and patient becomes even more pronounced: The shunt does not only influence the patient, but also adapts to the measured state of the patient. Up to now, analysis of this interdependence required *in vivo* experiments or was performed entirely *in silico* [22]. The former is closest to the clinical application, but is expensive, time-consuming, and raises ethical concerns. For these reasons, *in vivo* experiments are hardly used during the early development phases of new shunts. The latter approach is fast and cost-effective, but the behavior of the shunt has to be known precisely. Thus, numerical simulations are a good tool for developing concepts for new shunts, but *in vitro* or *in vivo* testing is still necessary for the hardware development.

Here we propose to combine an *in vitro* setup with mathematical modeling of the patient's relevant physiology to a hybrid test bed. This concept is referred to as hardware-in-the-loop (HIL) testing. It is commonly used during the

This work was supported by grants from the Swiss Academy of Engineering Sciences (2014-080), the 3R Research Foundation (140-14), and the Swiss National Science Foundation through NCCR Kidney.CH.

M. Gehlen is with the Institute for Dynamic Systems and Control, Department of Mechanical and Process Engineering, ETH Zurich, Zurich, Switzerland, and also with the Institute of Physiology, University of Zurich, Zurich, Switzerland (email: mgehlen@ethz.ch).

V. Kurtcuoglu is with the Institute of Physiology, and also the Neuroscience Center Zurich, and the Zurich Center for Integrative Human Physiology, University of Zurich, Zurich, Switzerland (email: vartan.kurtcuoglu@uzh.ch).

M. Schmid Daners is with the Product Development Group, Department of Mechanical and Process Engineering, ETH Zurich, Zurich, Switzerland (email: marischm@ethz.ch).

This paper has supplementary downloadable material available at http://ieeexplore.ieee.org, provided by the authors. This includes one multimedia MP4 format movie clip, which visualizes the test bed described in this manuscript. This material is 87.8 MB in size.

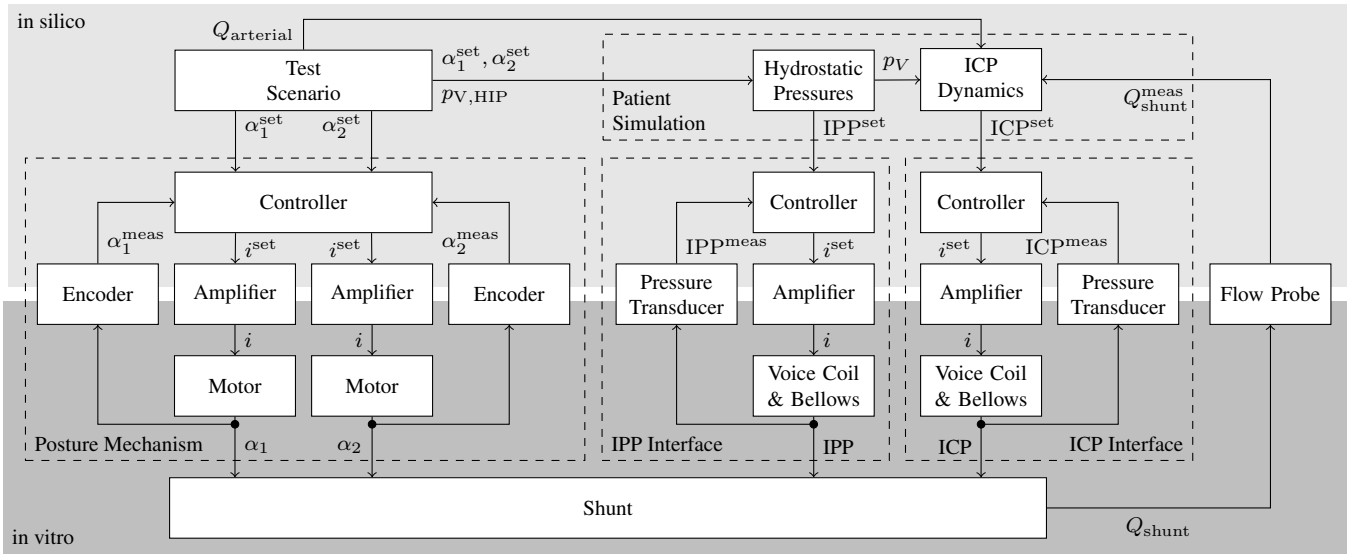

Fig. 1. Flow chart illustrating the interaction of software (in silico) and hardware (in vitro) parts of the hardware-in-the-loop setup: The basis of each experiment is a test scenario that determines the angles α_1 and α_2, venous pressure at the hydrostatic indifference point $p_{\mathrm{V,HIP}}$, and arterial inflow Q_{arterial}. The set values of α_1 and α_2 are applied to the shunt by the posture mechanisms as illustrated in Fig. 3. Based on the signals prescribed by the test scenario and the measured flow rate through the shunt $Q_{\mathrm{shunt}}^{\mathrm{meas}}$, the patient simulation determines the set values for ICP and IPP. ICP and IPP are then applied to the respective catheter ends by two pressure interfaces also shown in Fig. 2. The input current i for each of the actuators in the hardware-software interfaces is provided by an amplifier. The set values i^{set} for these amplifiers are determined by controllers, based on the measured signals α_1^{meas}, α_2^{meas}, $\mathrm{ICP}^{\mathrm{meas}}$, and $\mathrm{IPP}^{\mathrm{meas}}$ and their respective references (superscript set).

development of embedded systems [23] and combustion engines [24]. The method has also been applied successfully in the evaluation of ventricular assist devices [25]. Applied to the shunt test bed, the HIL concept implies that: 1) the patient's relevant physiology is replicated in real-time by a mathematical model; 2) the relevant simulated pressures for a ventriculoperitoneal CSF shunt (intracranial pressure (ICP) and intraperitoneal pressure (IPP)) are applied to the proximal and the distal ends of the drainage catheter; and 3) the drainage rate of CSF is measured and fed back to the *in silico* simulation in real-time.

In principle, any viable mathematical model of the patients physiology that yields the two necessary pressure signals as a function of the continuous measurement of the CSF drainage rate could be implemented. However, the necessity to interact with the hardware in real-time currently precludes complex computational fluid dynamics (CFD) simulations that can model the CSF dynamics in detail [26]. Thus, lumped parameter models are best suited. In 1973, Marmarou [27] published a lumped parameter model of the CSF dynamics whose parameters are even used to characterize hydrocephalus [28]. Today, there are a number of ICP models that build upon the exponential function of this model that describes the pressure dependence of the compliance and extend it to capture also other characteristics of the CSF system [29]. While the model of Marmarou describes the absolute compliance of the CSF system, which is defined relative to the ambient pressure, explicit modeling of the membranes between adjacent fluid compartments led to the concept of local compliances [30]. Some models are even representations of the whole body and include detailed descriptions of the cardiovascular system and its regulatory mechanisms [31]. However, most of these models assume that the patient is in supine position. To predict ICP of mobile patients, it is necessary to incorporate its posture dependence [32].

In the following, we describe a HIL test bed and investigate its suitability for analyzing the interdependence of shunt and patient dynamics and evaluating the performance of passive and active shunts during daily life situations including posture changes. The resulting drainage rates and ICPs are compared to a reference simulation without shunt and clinical results reported in literature.

II. Methods and Materials

A. General Concept

The test bed consists of an *in vitro* and an *in silico* domain (Fig. 1). Pressure interfaces link these two domains by applying simulated ICP and IPP to the respective ends of the catheter. A posture mechanism moves the shunt according to the current posture of the mimicked patient. The feedback loop is closed through a flow probe that measures the flow rate through the shunt and feeds this signal back into the patient simulation in real-time.

The patient model, all controllers and the data aquisition simultaneously run in a Real-Time Windows Target environment on a Windows 7 PC equipped with two data acquisition boards (MF634 and MF624 I/O cards, Humusoft s.r.o., Prague, Czech Republic). The code for the real-time environment is compiled from MATLAB/Simulink using an implicit fixed-step solver (ode14x) with a step size of 1 ms. This leads to a sampling rate of 1 kHz for all analog control and measured signals from and to the PC, while the drainage rate Q_{shunt} is transmitted through a digital connection and sampled at 100 Hz.

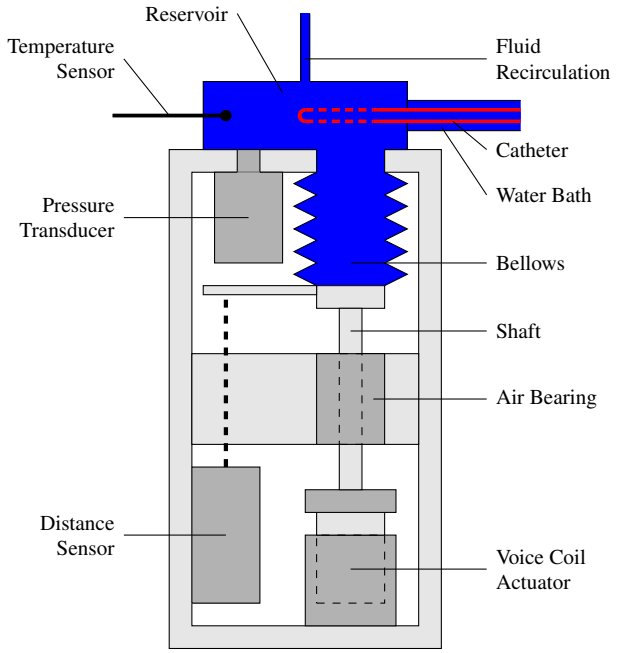

Fig. 2. Schematic drawing of the pressure interfaces that apply ICP and IPP calculated by the patient simulation to the respective ends of the catheter. In Fig. 1 and Fig. 3, they are identified as ICP and IPP interface, respectively. The reservoirs are pressurized by a voice coil actuator and feedback controlled through a ceramic pressure transducer. A distance sensor provides information on the fluid volume in the CSF reservoir.

B. Hardware-Software Interfaces

1) Intracranial and Intraperitoneal Pressure Interfaces: The pressures at the proximal and the distal ends of the catheter are applied through two pressure controlled fluid reservoirs (Fig. 2), each consisting of a rigid reservoir (polymethyl methacrylate) and a bellows (polytetrafluorethylene bellows, ElringKlinger Kunststofftechnik GmbH, Bietigheim-Bissingen, Germany) that is compressible in vertical direction [21]. The pressure in the reservoirs is controlled by varying the force applied to the bellows. The force is generated by a linear circular voice coil actuator (LVCM-051-064-01, MotiCont, Van Nuys, USA), which is powered by a 4-quadrant servo amplifier (ADS 50/10 4-Q-DC, Maxon Motor AG, Sachseln, Switzerland), and transferred through an air bearing (Air Bushing, New Way Air Bearings Inc.) supported shaft. This low friction actuation allows a resolution of 0.01 mmHg in the applied reservoir pressure. The reservoir pressure is measured by a piezo-resistive pressure sensor (PR-41X, Keller AG, Winterthur, Switzerland) with an accuracy of 0.1 mmHg and a resolution of 0.01 mmHg. The reservoir volume is computed from a laser-based measurement of the bellows position (optoNCDT 1700, Micro-Epsilon, Ortenburg, Germany). This volume information is used to regulate the recirculation of the test medium, which enables, in principle, infinite experiment duration. It further allows verification of the flow measurement.

2) Posture Mechanism: The patient's posture is simulated by moving the shunt and the aforementioned pressure interfaces with the mechanism shown in Fig. 3. The mechanism has two degrees of freedom that replicate rotational movements of the torso (α_1) and the head and neck (α_2). The beam lengths l_1 and l_2 are listed in Table I, where l_1 is the distance between waist and shoulder and l_2 between shoulder and eye height, which is close to the height of the external auditory canal usually used as the reference position for ICP measurements. Both values are based on [33] and correspond to the dimensions of a 50th-percentile 40-year-old American male. However, these lengths can be easily adapted to specific patients. The necessary torques to manipulate α_1 and α_2 are provided by two DC motors with planetary gearhead and integrated Encoder (RE 50, G52C 1:113, and HEDS 5540, Maxon Motors AG). These driving units are powered by 4-quadrant servo amplifiers (ESCON 50/5, Maxon Motors AG).

3) Flow Probe: The flow through the shunt is measured using a thermal MEMS sensor (SLI-2000, Sensirion AG, Staefa, Switzerland) with negligible hydrodynamic resistance (< 0.05 mmHg). The measurement signal is fed back to the patient simulation through an RS-232 connection at 100 Hz sampling rate.

TABLE I
CONSTANT PARAMETERS OF TEST BED AND PATIENT MODEL

Name	Value	Source
Q_{form}	0.35 mL/min	[30], [34]–[36]
R_{out} (physiologic)	8.57 mmHg/(mL/min)	[35], [36]
R_{out} (pathologic)	37.14 mmHg/(mL/min)	
$E_{\text{FV}} = E_{\text{BV}} = E^M$	0.1 1/mL	[21], [35], [36]
$p_{0,\text{FV}} = p_{0,\text{BV}} = \overline{p}_v$	7 mmHg	[36]
$p_{1,\text{FV}} = p_{1,\text{BV}} = p_b^M$	10 mmHg	[21], [30], [36]
$p_{\text{V,HIP}}$	7 mmHg	[32]
k_{BV}	0.35	
$k_{\text{FV}} = 1 - k_{\text{BV}}$	0.65	
R_{FB}	1 mmHg/(mL/min)	
Δh_{HIP}	33.8 cm	[32]
Δh_{jug}	11.0 cm	[32]
l_1	47.6 cm	[33]
l_2	16.5 cm	[33]

C. Patient Simulation

Fig. 4 outlines the lumped parameter model used in the following experiments. It is based on a four-compartment model developed by Stevens and Lakin [30], but modified and extended to include posture dependence, ICP pulsations, and visco-elastic effects.

1) Structure: Four fluid filled compartments - denoted F, B, A, and V - are used to model the patient's relevant physiology. Compartment F is the central CSF compartment that includes the ventricular system, the choroid plexus and the cranial and spinal subarachnoid space. This implicitly assumes equal pressure across the fluid spaces that are lumped into Compartment F. All viscoelastic effects within the craniospinal space are lumped into Compartment B (mainly brain tissue) that is connected to the main CSF space (F) through the constant resistance R_{FV}. The cerebral arteries and the cerebral and spinal veins are represented by the compartments A and V, respectively. The dynamics in each of these compartments are governed by a volume balance of all inflowing and outflowing

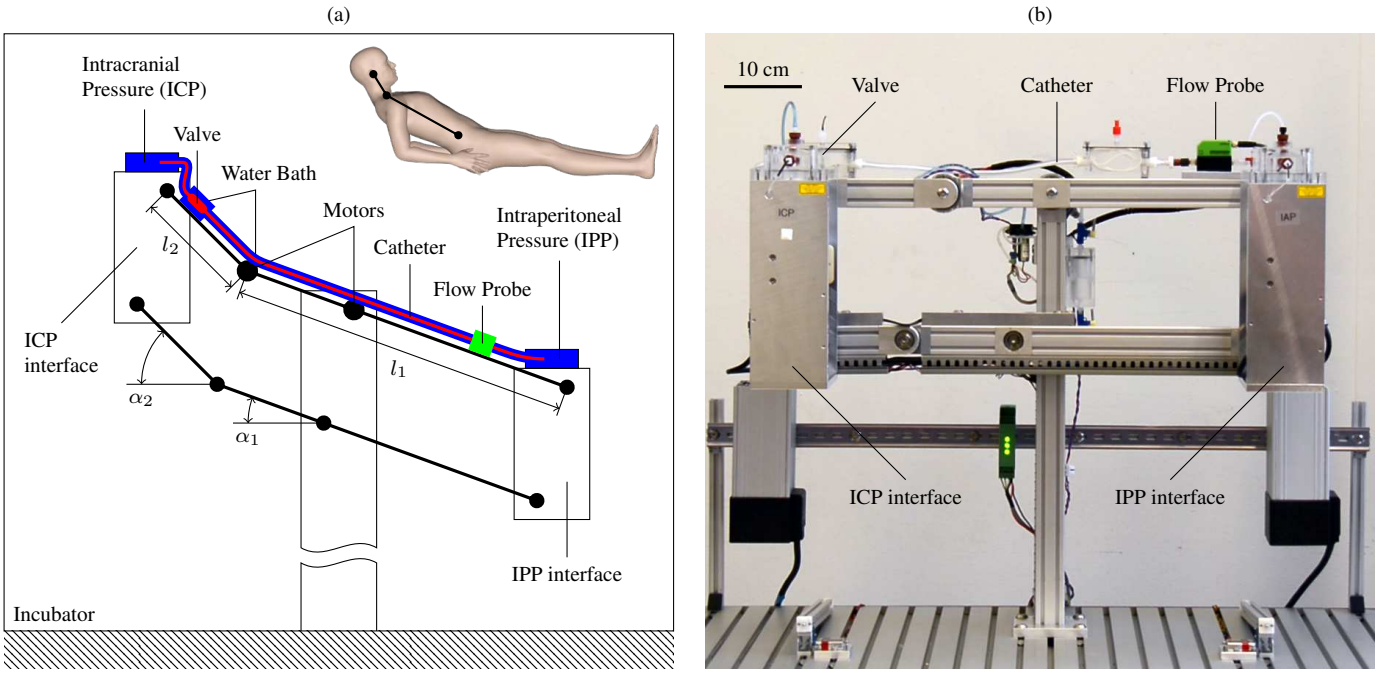

Fig. 3. Overview over the posture mechanism and the integration of the shunt into the system of pressure interfaces, water bath, and incubator. (a) Schematic with the posture mechanism mimicking the semirecumbent position shown in the upper right corner. l_1 and l_2 are the lengths of the two beams that represent the torso and the neck, respectively. Accordingly, α_1 and α_2 denote the orientations of these two beams with respect to the horizontal plane. A more detailed drawing of the ICP and IPP interfaces is shown in Fig. 2. (b) Picture of the test bed without the surrounding incubator in supine position. A movie of the test bed in action can be found in the supplementary materials.

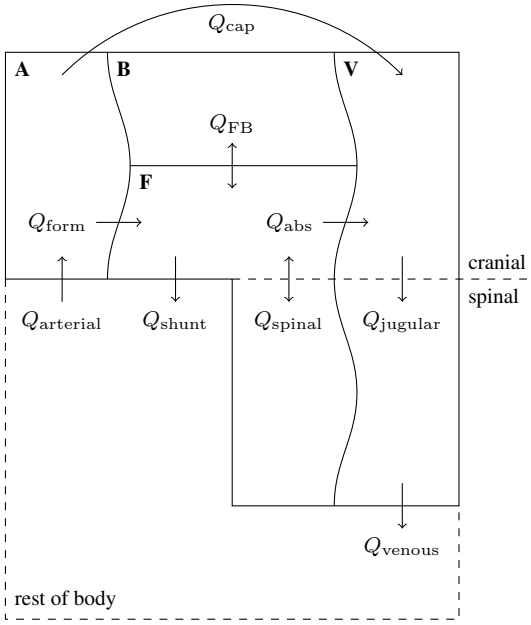

Fig. 4. Lumped parameter model that is used to simulate the relevant ICP dynamics (Fig. 1), which include the ventricular system and spinal canal (F), the brain tissue (B), the cerebral arteries (A), and the spinal and cerebral veins (V). Volume flows are denoted with Q_i and arrows indicate their usual direction. Wavy lines depict compliant vessel walls. Arterial inflow Q_{arterial}, venous pressure p_V, and the drainage rate Q_{shunt} as measured by the flow probe are inputs to this lumped parameter model. The main output is the CSF pressure p_F in Compartment F that is used as the ICP set value in the ICP interface.

volume flows Q and an additional algebraic equation that links the fluid volume V in the compartment to the fluid pressure p:

$$\frac{d}{dt}V_i(t) = -\sum_j Q_{\text{ij}}(p_i(t), p_j(t), t) \tag{1}$$

$$V_i(t) = \sum_j \Delta V_{\text{ij}}(p_i(t), p_j(t), t), \tag{2}$$

where t is time, i and j are indices referring to two interconnected compartments. The compliance function $\Delta V_{\text{ij}}(\cdot)$ describes the amount by which the volume of compartment i is increased and the one of compartment j is decreased or vice versa due to the pressure-dependent deformation of the boundary that separates the two fluid compartments i and j [30]. In contrast to the commonly used pressure based description, this volume based representation allows time-varying compliances and is more intuitive [37]. However, it turns the system of otherwise ordinary differential equations into a system of differential algebraic equations that is not guaranteed to be solvable in real-time.

2) Compliance: The global relationship between ICP and CSF volume is typically described by Marmarou's model [27], [35]:

$$p_{\text{IC}}^M = p_b^M e^{E^M \cdot \Delta V^M}, \tag{3}$$

which expresses ICP p_{IC}^M relative to ambient pressure as an exponential function of the added CSF volume ΔV^M, baseline pressure p_b^M, and the brain elastance coefficient E^M (Table I). The local compliance functions $\Delta V_{\text{ij}}(\cdot)$ introduced in (2) are chosen such that for slow volume changes ($p_F(t) \approx p_B(t)$)

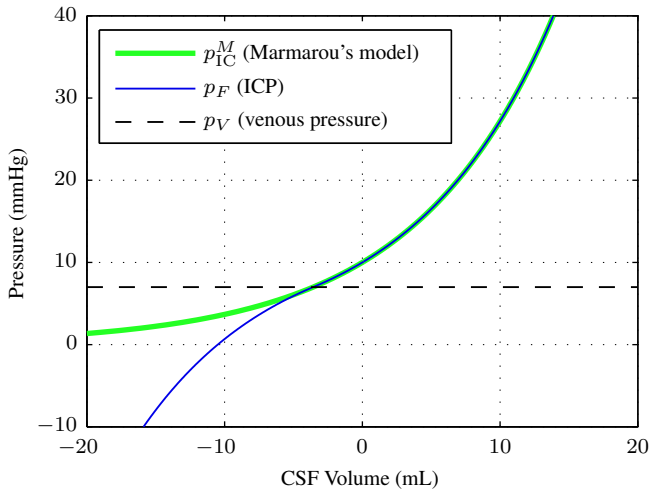

Fig. 5. Pressure-volume relationship of the patient model in steady state - implying equal pressures in Compartments B and F ($p_B = p_F$) - and for the cerebral venous pressure $p_V = 7\,\mathrm{mmHg}$ with respect to the total change in CSF volume ($\Delta V_{\mathrm{FV}} + \Delta V_{\mathrm{BV}}$). As a reference, the exponential compliance curve of Marmarou's model (3) is plotted for baseline pressure $p_b^M = 10\,\mathrm{mmHg}$ and brain elastance coefficient $E^M = 0.1\,1/\mathrm{mL}$, which are typical parameters for a healthy subject [36].

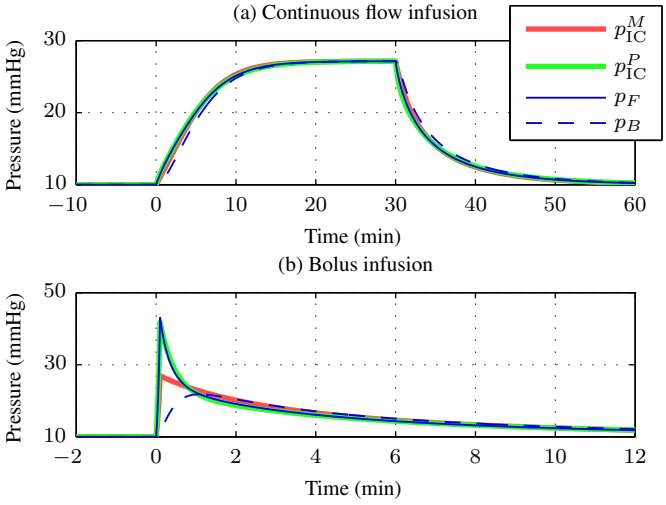

Fig. 6. Simulated response of pressures p_F and p_B in the compartments F and B, respectively, to infusions into compartment F. The results are compared to the ICPs p_{IC}^M and p_{IC}^P calculated with Marmarou's model [27] and the viscoelastic model introduced by Bottan et. al. [36], respectively. (a) Continuous flow infusion (constant infusion rate of 1.5 mL/min between $t = 0$ and 30 min). (b) Bolus infusion (infusion of 10 mL between $t = 0$ and 0.1 min).

and $p_F(t) \geq p_V(t)$ the global pressure-volume relationship of the patient model is equivalent to the original Marmarou model (Fig. 5):

$$\Delta V_{\mathrm{ij}}(t) = \begin{cases} \frac{k_{\mathrm{ij}}}{E_{\mathrm{ij}}} \cdot \ln \frac{p_i(t)-p_j(t)+p_{0,\mathrm{ij}}}{p_{1,\mathrm{ij}}}, & \text{for } p_i(t) \geq p_j(t) \\ \frac{k_{\mathrm{ij}}}{E_{\mathrm{ij}}} \cdot (2 \cdot \ln \frac{p_{0,\mathrm{ij}}}{p_{1,\mathrm{ij}}} - \ln \frac{p_j(t)-p_i(t)+p_{0,\mathrm{ij}}}{p_{1,\mathrm{ij}}}), & \text{for } p_i(t) < p_j(t) \end{cases} \tag{4}$$

for the parameters listed in Table I. The resulting pressure-volume relationship is inverted for reversed pressure gradients (Fig. 5). A similar S-shape of this global pressure-volume relationship was observed in vivo [38], [39] and it can explain negative ICP as it occurs following excessive drainage [30], [40].

3) CSF Formation and Absorption: The overall rate of CSF formation Q_{form} is assumed constant [34], [35], [41]. While the relative contribution of the different sites of CSF absorption are still being researched, it appears clear that the arachnoid granulations are a major pathway; the overall outflow is thus positive and depends linearly on the hydrostatic pressure gradient [34], [35]:

$$Q_{\mathrm{abs}} = \begin{cases} (p_F - p_V)/R_{\mathrm{out}}, & \text{for } p_F \geq p_V \\ 0, & \text{for } p_F < p_V \end{cases} \tag{5}$$

In case of shunting, an additional CSF flow Q_{shunt} is diverted from compartment F. Q_{shunt} is an input to the mathematical model and its actual value originates from the flow probe, which measures the flow rate through the tested shunt *in vitro* (Fig. 1).

4) Brain Compartment: From an anatomical point of view, the compartment B represents the brain tissue and peripheral parts of the CSF system. It allows for modeling of the viscoelastic response that is e.g. observed during bolus infusions [36]. The effects that may be responsible for this behavior entail limited wave propagation speeds between distant locations of the CSF space [42], fluid exchange between CSF and interstitial fluid [43], and the viscoelastic mechanical response of the brain tissue [44], [45]. For a simplified model with constant compliances, it can be shown that with $R_{\mathrm{FB}} = 1\,\mathrm{mmHg/(mL/min)}$ and $k_{\mathrm{BV}} = 0.35$ this lumped compartment approach is equivalent to the model of Bottan et. al. [36] (Fig. 6). Their model is an extended version of Marmarou's model that uses a Prony series to map the viscoelastic effects and showed good accordance with measured infusion tests.

5) Cardiovascular System and Posture: While the cardiovascular system greatly influences the intracranial dynamics, the blood flows are hardly altered by the CSF production or absorption due to the in comparison negligible flow rates. Therefore, the arterial inflow is a given input to the system and any theoretical or measured flow function can be applied. Since pulsations in the intracranial fluid system, which are introduced through the cardiac action, play an important role in the distribution of CSF and, more importantly, can alter the drainage rates through the shunt [12], we use a periodic pulsating arterial flow function for Q_{arterial}. The values of this function are based on phase contrast magnetic resonance imaging of the internal carotid artery in 94 elderly patients (68 ± 8 years of age) [46].

Compared to the pulsatile flow component of arteries, pulsatility of capillary vessels is small. The blood flow through the capillaries Q_{cap} is thus assumed to be non-pulsatile. Its value is given by the volume balance:

$$Q_{\mathrm{cap}} = \overline{Q}_{\mathrm{arterial}} - Q_{\mathrm{form}} \tag{6}$$

where $\overline{Q}_{\mathrm{arterial}}$ is the mean arterial flow over one cardiac cycle and Q_{form} is the constant rate of CSF formation. Therefore, the volume of the blood in compartment A is modeled independent

of any pressure. Since the cerebral artery pressure p_A is much higher than the pressures p_F and p_B in the compartments F and B at all times, one can assume a constant ratio between ΔV_{AB} and ΔV_{AF}, which then simplifies the patient model to a system of ordinary differential equations. Further assuming that the ratio of arterial to venous blood vessels is the same at the boundaries of the compartments F and B leads to

$$\Delta V_{\mathrm{AB}}(t)/\Delta V_{\mathrm{AF}}(t) = k_{\mathrm{BV}}/k_{\mathrm{FV}}. \tag{7}$$

On the venous side, the system boundary is defined by a non-pulsatile venous pressure, which depends on the patient's posture. This posture dependence is implemented using the concept of a hydrostatic indifference point in the venous system and taking collapsible jugular veins into account when calculating the hydrostatic pressure component of the cerebral venous pressure p_V [32]:

$$p_V = \begin{cases} p_{\mathrm{V,HIP}} - \Delta p_{\mathrm{HIP}}, & \text{for } p_{\mathrm{V,HIP}} \geq \Delta p_{\mathrm{HIP}} - \Delta p_{\mathrm{jug}} \\ -\Delta p_{\mathrm{jug}}, & \text{for } p_{\mathrm{V,HIP}} < \Delta p_{\mathrm{HIP}} - \Delta p_{\mathrm{jug}} \end{cases} \tag{8}$$

where $p_{\mathrm{V,HIP}}$ is the pressure in the hydrostatic indifference point (HIP) of the venous system, Δp_{HIP} the hydrostatic pressure difference in blood between the lateral ventricles and the HIP, and Δp_{jug} between the lateral ventricles and the jugular veins. In the HIL setup, Δp_{HIP} and Δp_{jug} are functions of the angles α_1 and α_2:

$$\Delta p_{\mathrm{HIP}} = \rho \cdot g \cdot (l_2 \cdot \sin\alpha_2 + (\Delta h_{\mathrm{HIP}} - l_2) \cdot \sin\alpha_1) \tag{9}$$

$$\Delta p_{\mathrm{jug}} = \rho \cdot g \cdot \Delta h_{\mathrm{jug}} \cdot \sin\alpha_2 \tag{10}$$

Due to the concept of local compliances, the posture dependent cerebral venous pressure p_V has an immediate effect on the pressures in the adjacent compartments p_F and p_B.

D. Shunt

In principle, any CSF shunt can be tested with the presented test bed. For the purpose of analyzing and validating the HIL setup, three identical ball and cone valves (miniNAV, Christoph Miethke GmbH & Co. KG, Potsdam, Germany) with $7.4\,\mathrm{mmHg}$ ($10\,\mathrm{cmH_20}$) opening pressure are used. In the following, the three valves will be denoted as Valve No. 1, 2, and 3. In one experiment, Valve No. 1 is complemented by a gravitational unit (proSA, Christoph Miethke GmbH & Co. KG, Potsdam, Germany) that has $0\,\mathrm{mmHg}$ opening pressure in horizontal orientation and is set to $14.7\,\mathrm{mmHg}$ ($20\,\mathrm{cmH_2O}$) opening pressure in upright orientation. The valve and, if used, the gravitational unit are connected to the pressure interfaces through catheters with $1.2\,\mathrm{mm}$ inner diameter. The catheter lengths from the ICP interface to the valve and from the valve to the IPP interface are $20\,\mathrm{cm}$ and $84\,\mathrm{cm}$, respectively.

E. Test Medium and Ambient Conditions

The test medium, which imitates CSF, is deionized and deaerated water. The valve and both catheters are submerged in a water bath filled with the same medium (Fig. 3).

The entire *in vitro* setup is enclosed within an incubator kept at $37\pm1\,^{\circ}\mathrm{C}$, which equals the tissue temperature at the typical implantation site of the valve and fulfills the requirements mandated by the standards BS EN ISO 7197:2009 and ASTM F647-94(2006). This is done through two feedback controlled fan heaters (HGL 046 - 400 W, Stego Elektrotechnik GmbH, Germany). Continuous temperature measurements are taken using $10\,\mathrm{kOhm}$ NTC Thermistors (BetaCurve Interchangeable Thermistor, BetaTHERM Sensors, Galway, Ireland) at 5 locations: 1) in the ICP reservoir; 2) in the IPP reservoir; 3) in the water bath next to the valve; 4) in the air inside the incubator; and 5) in the ambient air outside of the incubator.

TABLE II
MODELING OF RELEVANT POSTURES AND DAILY ACTIVITIES

Activity	Modeling	Source
lying (supine)	$\mathrm{IPP} = 1.8\,\mathrm{mmHg}$, $\alpha_1 = \alpha_2 = 0^{\circ}$	[47]
sitting	$\mathrm{IPP} = 16.7\,\mathrm{mmHg}$, $\alpha_1 = \alpha_2 = 90^{\circ}$	[47]
standing	$\mathrm{IPP} = 20.0\,\mathrm{mmHg}$, $\alpha_1 = \alpha_2 = 90^{\circ}$	[47]
sitting up	gradual trunk (α_1) and head (α_2) movement	[49]
lying down	reversed sit-up movement	
coughing	simultaneous increase in IPP and $p_{\mathrm{V,HIP}}$ by up to $68\,\mathrm{mmHg}$ and $43\,\mathrm{mmHg}$, respectively	[50]

F. Experiments

Initial three sets of experiments were performed to validate the proposed shunt test bed, to analyze the interaction between shunt and patient, and to study how this interaction is changed upon inclusion of a gravitational unit. This was examined in a synthetic situation where overdrainage would occur *in vivo*, as well as during a 24-hour period that resembles a typical day of a patient.

Experiment 1 (Shunt Characteristic): The shunts' pressure-flow characteristics during opening and closing of the valve were determined by measuring the flow through the shunt while linearly increasing the pressure difference between the proximal and the distal ends of the catheter from 0 to $30\,\mathrm{mmHg}$ within $2\,\mathrm{mins}$, and then linearly decreasing it back to $0\,\mathrm{mmHg}$ at the same rate. The experiment was performed twice before and twice after each of the other experiments: once with the postural mechanism in horizontal position ($\alpha_1 = \alpha_2 = 0^{\circ}$) and once in upright position ($\alpha_1 = \alpha_2 = 90^{\circ}$). While ICP changed continuously during this experiment, IPP was kept constant at $1.8\,\mathrm{mmHg}$ and $16.7\,\mathrm{mmHg}$ for the experiment in horizontal and upright position, respectively. These are realistic IPP values for subjects in supine and sitting position [47], [48].

Experiment 2 (Synthetic Posture Change): The setup's ability to mimic postural changes and posture related overdrainage was tested by simulating a patient who quickly moves (within $5\,\mathrm{s}$) from supine position to sitting and then goes back to supine position again (Table II). Each of the three postures was held for $1\,\mathrm{hour}$ to guarantee equilibrium conditions at the end of each period. The transitions were gradual changes of α_1, α_2 and IPP. The initial state of the patient simulation was the equilibrium state without shunting ($p_F = p_B = 10\,\mathrm{mmHg}$). In addition to the physiological case with $R_{\mathrm{out}} = 8.57\,\mathrm{mmHg}$,

the experiment was also repeated for a pathological case with an elevated CSF outflow resistance of 37.14 mmHg, which corresponds to a patient with an ICP of 20 mmHg in supine position without shunting. The experiment was repeated three times for each valve combination. Experiment 2 was also used to quantify the performance of the pressure interfaces. This was done by comparing the desired and measured pressures in the ICP interface, where the ICP pulsations pose high dynamic requirements for the pressure control.

Experiment 3 (Daily Routine): The idea behind the third experiment is that for future smart and active shunts it will not be sufficient to only consider the static characteristic of the valve, because the valve will adapt to the patient. Therefore, we need a new means to assess and compare the performance of these new devices. One promising approach to this problem is to define a scenario that resembles the daily routine of the targeted patient or patient group most realistically. This idea can be compared to the driving cycles that are used to estimate the fuel consumption and emissions of a given car or truck within a typical environment [51], [52]. We generated a cycle from a case study of a subject's daily routine that was recorded over 24 hours [50] consisting of the postures and activities listed in Table II. While this cycle cannot be considered to be representative, it does serve its purpose of providing a proof of principle. Valve No. 1 with and without the gravitational unit was used in connection with the pathologic case for this cycle. The ICP of a healthy subject (physiologic outflow resistance) without a shunt was simulated as a benchmark to which the ICP recorded during the cycle was compared.

III. Results

All recordings of the experiments were filtered with a second-order zero-phase Butterworth filter with 50 Hz cutoff frequency using the MATLAB function filtfilt. Results that are based on multiple measurements are given as mean values ± standard deviation.

Experiment 1 (Shunt Characteristic)

The pressure-flow characteristics of the tested valves are depicted in Fig. 7, and their measured opening pressures are listed in Table III. The valve manufacturer defines the opening pressure as the pressure necessary to obtain a drainage rate of 0.083 mL/min (5 mL/h). According to this definition, the measured opening pressure over the valve, both catheters and the flow sensor is 7.17 ± 1.02 mmHg (measurements on the three separate ball and cone valves of the same type). The nominal opening pressure for the valves without catheters is 7.4 mmHg (10 cmH_2O). Adding the gravitational unit to one of the ball and cone valves (Valve No. 1) does not change the measured opening pressure of this valve in supine position notably. It does, however, increase flow resistance above the opening pressure (Fig. 7b) and it increases the opening pressure in upright position to 16.98 ± 1.05 mmHg (Table III).

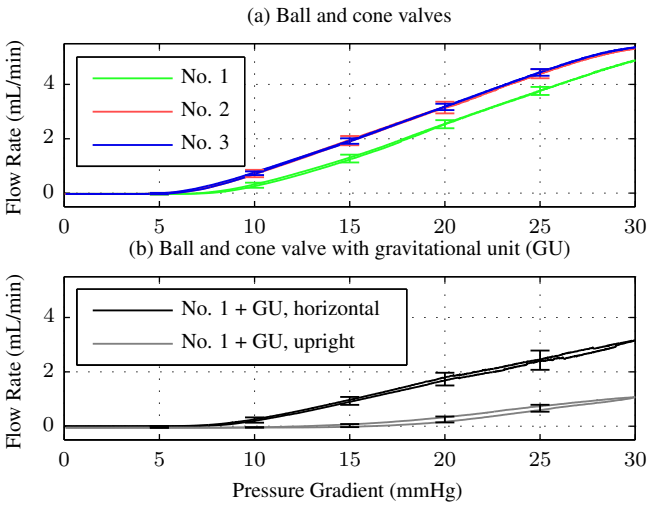

Fig. 7. Experiment 1: Pressure-flow characteristics during opening and closing of the tested valves. The curves represent mean values over four repetitions of Experiment 1 in horizontal position and four repetitions in upright position. Error bars indicate the standard deviations at 5, 10, 15, 20, and 25 mmHg. (a) Ball and cone valves No. 1-3. (b) Valve No. 1 combined with the gravitational unit (GU) with separate curves for horizontal and upright position.

Experiment 2 (Synthetic Posture Change)

Experiment 2 shows how the drainage rate and ICP evolves when a patient sits up or lies down, and how this behavior is affected by the addition of a gravitational unit to the ball and cone valve. As an example, Fig. 8 shows the ICP and flow rate through the shunt for one iteration of the experiment and compares the measurements to reference values obtained by simulation without shunt. In this reference case, mean ICP is 10.00 mmHg in supine position. In sitting position, the proximal catheter tip rises above the CSF system's point of hydrostatic indifference. This posture-induced reduction in the hydrostatic pressure at the ICP reference point leads to negative mean ICP (−5.10 mmHg) relative to ambient pressure [32]. The corresponding movements of the posture mechanism are visualized in a video clip accompanying this manuscript. We use the equilibrium conditions in supine and sitting posture and the time it takes to reach these to quantify the experimental results. The equilibrium values are averaged over the periods 20 min $< t <$ 60 min and 80 min $< t <$ 120 min for supine and sitting position, respectively. In the following, we consider equilibrium to have reached when the mean ICP is and stays within 1 mmHg of this value.

1) Physiological Case: For the physiological case with $R_{\text{out}} = 8.57$ mmHg/(mL/min) and supine position, the shunt decreases ICP from 10 mmHg (reference case, no shunt) to 9.10 ± 0.38 mmHg. After sitting up, ICP instantaneously falls to -6.24 ± 0.36 mmHg due to the increased hydrostatic pressure difference. However, this fall in ICP and the modeled increase in IPP (from 1.8 mmHg to 16.7 mmHg) does not fully compensate the hydrostatic water column in the catheter, which leads to a maximum drainage rate of 4.41 ± 0.20 mL/min (averaged over one cardiac cycle). Equilibrium is reached after 9.21 ± 1.49 min at ICP of -21.06 ± 1.34 mmHg. The patient's recovery from this

TABLE III
MEAN VALUES AND PEAK-TO-PEAK AMPLITUDES OF ICP AND SHUNT FLOW AFTER STEADY STATE WAS REACHED DURING EXPERIMENT 2.

			ICP (mmHg)		Shunt Flow (mL/min)	
Posture	Valve	Opening Pressure (mmHg)	mean	amplitude	mean	amplitude
Supine	no shunt		10.00	1.14	0.00	0.00
	No. 1	8.34 ± 0.32	9.60 ± 0.08	1.09 ± 0.01	0.05 ± 0.01	0.04 ± 0.01
	No. 2	6.65 ± 0.39	8.82 ± 0.08	1.01 ± 0.01	0.14 ± 0.01	0.06 ± 0.02
	No. 3	6.47 ± 0.11	8.89 ± 0.02	1.01 ± 0.00	0.13 ± 0.00	0.06 ± 0.01
	No. 1 + grav. unit	8.54 ± 0.80	9.69 ± 0.04	1.10 ± 0.00	0.03 ± 0.00	0.02 ± 0.00
	No. 1 (increased R_{out})	8.29 ± 0.46	11.61 ± 0.48	1.32 ± 0.05	0.22 ± 0.01	0.13 ± 0.01
Sitting	no shunt		-5.10	1.14	0.00	0.00
	No. 1	8.62 ± 0.64	-19.36 ± 0.33	2.14 ± 0.04	0.35 ± 0.01	0.35 ± 0.01
	No. 2	6.52 ± 0.62	-21.68 ± 0.62	2.41 ± 0.07	0.34 ± 0.01	0.38 ± 0.03
	No. 3	6.44 ± 0.10	-22.15 ± 0.03	2.47 ± 0.00	0.35 ± 0.00	0.39 ± 0.01
	No. 1 + grav. unit	16.98 ± 1.05	-9.07 ± 0.06	0.94 ± 0.01	0.35 ± 0.02	0.04 ± 0.00
	No. 1 (increased R_{out})	8.12 ± 0.30	-20.25 ± 0.51	2.24 ± 0.06	0.35 ± 0.00	0.30 ± 0.06

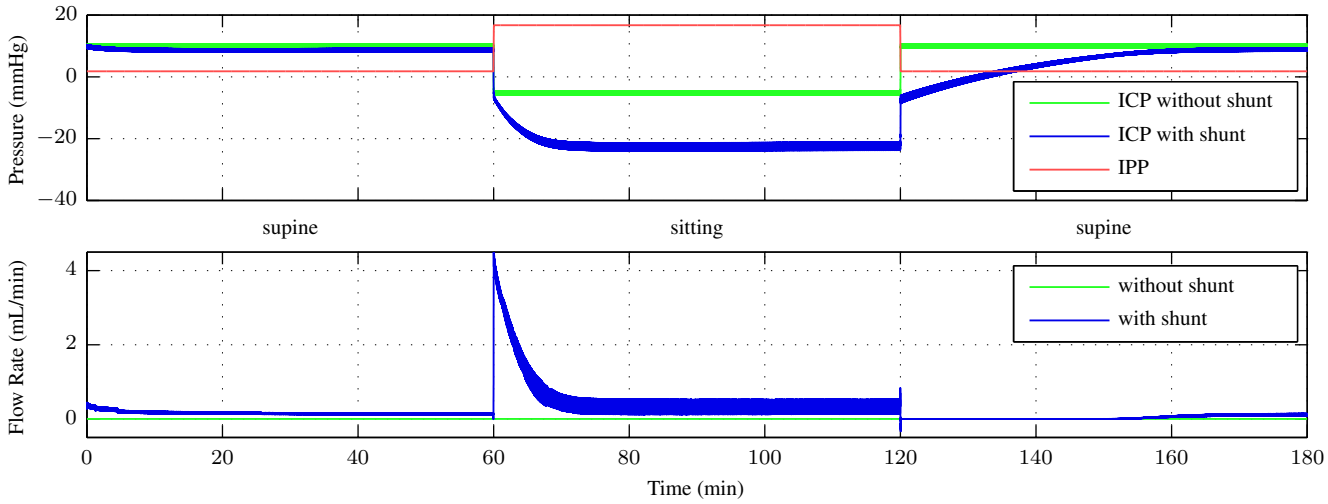

Fig. 8. Experiment 2: Simulation of a patient with physiological outflow resistance of $R_{\text{out}} = 8.57\,\text{mmHg/(mL/min)}$ and an implanted ball and cone valve (Valve No. 2). The patient sits up from supine position at $t = 60\,\text{min}$ and lies back down at $t = 120\,\text{min}$. As a reference, the experiment is plotted for the same patient without shunt. The signals are plotted with $0.1\,\text{s}$ sampling time, thus the line widths are proportional to the amplitude of the signal pulsations. Two zoomed segments of this plot, which give detailed views of the effect of vasculature pulsation, are shown in Fig. 9.

overdrainage is slower and takes $34.68 \pm 1.12\,\text{min}$.

A metric that gives an indication of the patient's current compliance is the amplitude of the ICP pulsations. In the reference case, the peak-to-peak amplitude is $1.14\,\text{mmHg}$ independent of the patient's posture. With the shunt, this decreases slightly to $1.04 \pm 0.04\,\text{mmHg}$ for the supine position and increases to $2.34 \pm 0.16\,\text{mmHg}$ while sitting.

2) Pathological Case: When conducting the same experiment, but with increased outflow resistance, ICP is only decreased to $11.61 \pm 0.48\,\text{mmHg}$ in supine position while diverting $0.22 \pm 0.01\,\text{mL/min}$ through the shunt. The overdrainage in the sitting posture ($0.35 \pm 0.00\,\text{mL/min}$) still leads to an equilibrium ICP of $-20.25 \pm 0.51\,\text{mmHg}$. As expected, the difference to the physiological case is small here, because the resulting ICP is below the cerebral venous pressure p_V ($-8.10\,\text{mmHg}$ in sitting posture). Therefore, the entire CSF production ($0.35\,\text{mL/min}$) is diverted through the shunt in both cases.

3) Gravitational Valve: Adding a gravitational unit to the valve does not change the equilibrium ICP in the supine position notably ($9.69 \pm 0.04\,\text{mmHg}$). During the sitting phase of the experiment, all of the CSF produced is still drained through the shunt. The ICP, however, is only lowered to $-9.07 \pm 0.06\,\text{mmHg}$, which also keeps the ICP pulsations ($0.94 \pm 0.01\,\text{mmHg}$) closer to the reference scenario.

4) Pressure Control: For Experiment 2, Fig. 9 compares within a time window of three seconds the pulsatile ICP values prescribed by the *in silico* domain with the ICP measured in the reservoir of the ICP interface. The mean absolute error (MAE) in the interface is $0.075\,\text{mmHg}$ over all experiments. The maximum absolute error stays below $1\,\text{mmHg}$ in all experiments. After compensating for the delay of $25\,\text{ms}$ between the *in silico* and the *in vitro* domains, the MAE decreases to $0.007\,\text{mmHg}$. For the IPP interface, the MAE is $0.027\,\text{mmHg}$. Compensating for the delay does not significantly change the error here, because the reference signal for this compartment

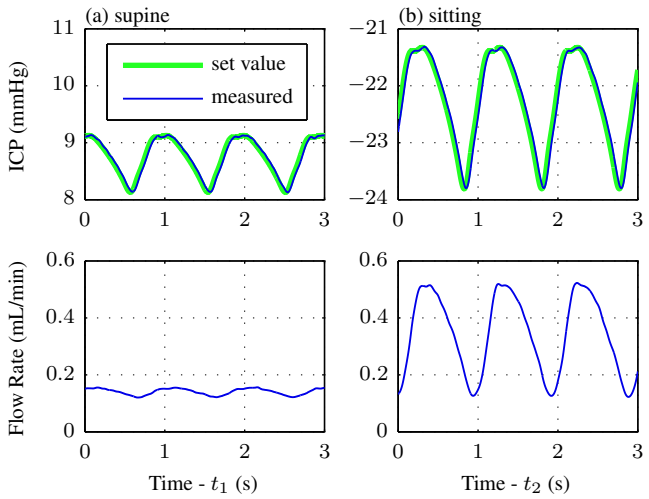

Fig. 9. Comparison between set (by the *in silico* domain) and measured (in the *in vitro* domain) ICP values in Experiment 2 presented in Fig. 8. The bottom panels show the corresponding measured pulsatile drainage rate. (a) Supine position: Time window starts at $t_1 = 40$ min into the experiment. (b) Sitting: Time window starts at $t_2 = 100$ min.

is not pulsatile.

Experiment 3 (Daily Routine)

Fig. 10 depicts the results of Experiment 3 carried out with valve No. 1, without the gravitational unit. At nighttime, the simulated patient is in supine position, and the ICP stabilizes around the equilibrium ICP in supine position that was determined in the synthetic posture change experiment. At daytime, the patient is mainly sitting or standing. There are numerous transitions between these postures. Therefore, the simulated IPP alternates between 16.7 mmHg and 20 mmHg, while the vertical distance between the proximal and the distal end of the catheter remains constant. In the reference simulation, which mimics a healthy subject without shunt, the mean ICP is -5.10 mmHg in sitting or standing position. The behavior of the shunted patient is different in two ways: First, overdrainage occurs and low ICP values as measured in Experiment 2 can be observed. Second, CSF drainage rate and with it ICP are directly dependent on IPP. This means that the ICP in standing position is higher than in sitting position. Adding a gravitational unit hardly influences ICP at nighttime, but reduces overdrainage while the patient is sitting or standing. The pressure spikes in Fig. 10 are the result of coughing, which is modeled as outlined in Table II. These pressure peaks result in mainly negative spikes in the measured flow rate, which will cause the valve to close. However, they do not have any significant and prolonged effect on the ICP. Over the entire 24-hours cycle, the mean absolute difference in ICP between shunted patient and healthy subject is 9.16 mmHg without gravitational unit and 2.29 mmHg with.

IV. Discussion

The results presented at hand demonstrate that the HIL test bed can be used to study the static and dynamic properties of CSF shunts, and their interaction with the patient.

The opening pressures and characteristics obtained in Experiment 1 compare well with the manufacturer's specifications, but also show marked differences between the measured mean opening pressures of valve No. 1 and the remaining two valves, which are larger than the experiments' standard deviations.

In Experiment 2, we were able to reproduce the problem of overdrainage when using a standard differential pressure valve, and observe how the addition of a gravitational unit can prevent it. The high measured flow rates and the subsequent fall in ICP are in good agreement with the literature [8].

In the same experiment, we observed that in supine position the valves start continuously draining before the difference between mean ICP and IPP rises above the valve's opening pressure (Fig. 9). While it is known that the apparent opening pressure is lowered in the presence of pressure pulsations [12], it was assumed that CSF is only drained during the pressure peaks. The continuous flow in our experiment might be due to a hysteresis in the valve opening. This result highlights that the drainage is influenced by ICP pulsations; these should thus be taken into account when testing CSF shunts.

We know from *in vivo* studies that the amplitude of ICP pulsations increases with elevated mean ICP and can be decreased through shunting until a certain minimum amplitude [53], [54]. In supine position, we can reproduce the reduction in ICP pulse amplitude with all shunts. In sitting position, however, the amplitude is only decreased with the gravitational unit. For the very low ICP values that are reached during overdrainage, we measure even higher amplitudes than without shunting, which is due to the symmetry of the compliance curve around the venous pressure (Fig. 5). A similar amplitude increase at negative ICP has been observed after withdrawal of CSF in dogs [40], [55].

Experiment 2 further proves that the feedback controllers of the critical pressure interfaces are able to follow the respective reference curves precisely. The interfaces can apply any pathophysiologic pulse waveform or pressure spike to the shunt. The delay that is introduced by the controlling feedback loop is small. It is even irrelevant when looking at periodically pulsating signals.

The cycle simulated in Experiment 3 is only based on the recordings of one subject, and should thus not be considered representative of any subpopulation of hydrocephalus patients. The experiment does, however, demonstrate the feasibility of simulating an arbitrary daily routine for a period of 24 hours or longer. By comparing the simulated ICPs of such an experiment to a reference simulation, we can provide a simple metric that quantifies the performance of CSF shunts for a realistic scenario. The two results of the shunt with and without the gravitational unit suggest that the metric is sensitive to improvements in shunt technology. In contrast to measurements of the shunt's pressure-flow characteristic, the results will even be meaningful for active shunts that adapt to the posture of the patient, mean ICP or the ICP pulse waveform.

Compared to pure *in vitro* implementations, the main advantages of the HIL approach used for our setup are the flexibility of the patient model and its determinism: The simulated patient or the severity of the pathology can be changed by adjusting

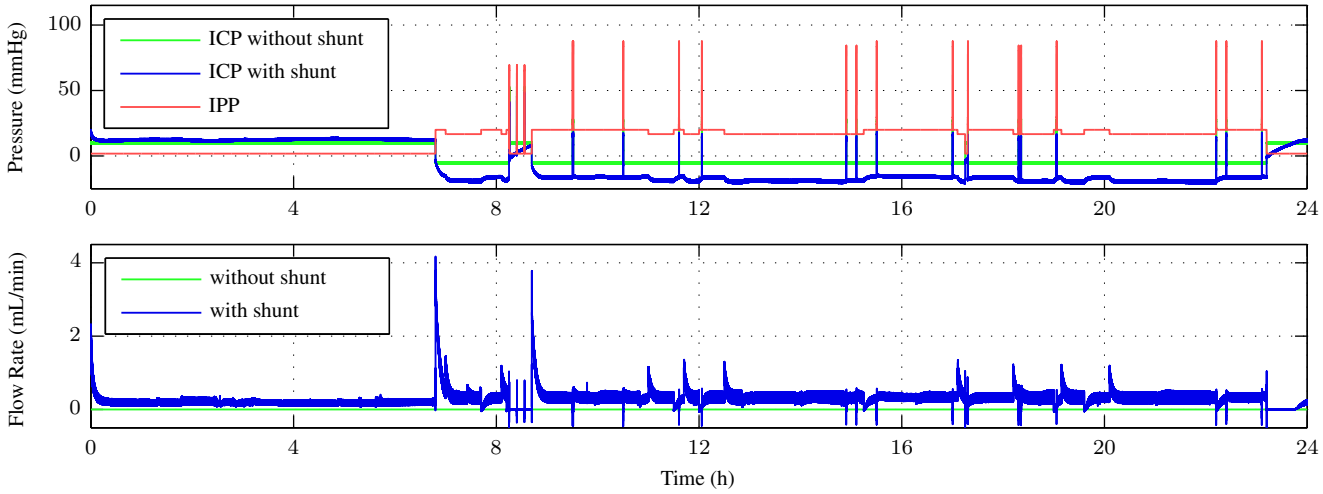

Fig. 10. Experiment 3: Simulation of a shunted patient's routine activities over a 24-hour period. The patient has increased outflow resistance. No gravitational unit is implanted. As a reference, the same activities of a healthy, not shunted subject with physiological outflow resistance are simulated. The signals are plotted with 0.1 s sampling time, thus the line widths are proportional to the amplitude of the signal pulsations.

the model parameters. Sets of parameters representing specific patients or patient groups can at least in part be derived from available clinical data such as ICP recordings during lumbar infusions tests. Physiologic and pathophysiologic increases in abdominal pressure as they occur, respectively, during pregnancy and due to obesity can be taken into account by increasing mean IPP. Finally, HIL testing can be extended to ventriculoatrial and ventriculopleural shunts by adapting the posture mechanism and patient model.

V. Conclusion

Our test bed can be used to quantify and assess the expected performance of passive and active shunts in a realistic environment. The HIL approach on which the test bed is based does not only provide a means of comparison for existing shunts; it can also stimulate the development of smart and active shunts by lowering the burden of implementing and testing new concepts and ideas. In combination with comprehensive and well specified test cycles, we can imagine the application of HIL testing during the regulatory approval process of new devices.

Acknowledgment

The authors would like to thank M. Hubacher, D. Wagner and D. Brühlmann for their work on the test bed, and T. Vasileiou for his spadework. The tested valves were provided by Christoph Miethke GmbH & Co. KG (Potsdam, Germany).

References

[1] H. L. Rekate, "The definition and classification of hydrocephalus: a personal recommendation to stimulate debate," *Cerebrospinal Fluid Research*, vol. 5, no. 1, p. 2, 2008.

[2] R. D. Adams *et al.*, "Symptomatic occult hydrocephalus with normal cerebrospinal-fluid pressure: a treatable syndrome," *New England Journal of Medicine*, vol. 273, no. 3, pp. 117–126, Jul 1965.

[3] A. Aschoff *et al.*, "The scientific history of hydrocephalus and its treatment," *Neurosurg. Rev.*, vol. 22, no. 2, pp. 67–93, 1999.

[4] J. Kestle *et al.*, "Long-term follow-up data from the shunt design trial," *Pediatric Neurosurgery*, vol. 33, no. 5, pp. 230–236, 2000.

[5] S. R. Browd *et al.*, "Failure of cerebrospinal fluid shunts: part I: obstruction and mechanical failure," *Pediatric Neurology*, vol. 34, no. 2, pp. 83–92, Feb 2006.

[6] ——, "Failure of cerebrospinal fluid shunts: part II: overdrainage, loculation, and abdominal complications," *Pediatric Neurology*, vol. 34, no. 3, pp. 171–176, Mar 2006.

[7] B. R. Lutz *et al.*, "New and improved ways to treat hydrocephalus: Pursuit of a smart shunt," *Surgical Neurology International*, vol. 4, no. 2, p. 38, 2013.

[8] A. Aschoff *et al.*, "Overdrainage and shunt technology, a critical comparison of programmable, hydrostatic and variable-resistance valves and flow-reducing devices," *Child's Nervous System*, vol. 11, no. 4, pp. 193–202, Apr 1995.

[9] Z. Czosnyka *et al.*, "Posture-related overdrainage: Comparison of the performance of 10 hydrocephalus shunts in vitro," *Neurosurgery*, vol. 42, no. 2, pp. 327–333, Feb 1998.

[10] ——, "Laboratory testing of hydrocephalus shunts - conclusion of the u.k. shunt evaluation programme," *Acta Neurochirurgica*, vol. 144, no. 6, pp. 525–538, Jun 2002.

[11] ——, "Evaluation of three new models of hydrocephalus shunts." *Acta neurochirurgica. Supplement*, vol. 95, p. 223, 2005.

[12] ——, "Hydrocephalus shunts and waves of intracranial pressure," *Medical and Biological Engineering and Computing*, vol. 43, no. 1, pp. 71–77, 2005.

[13] A. Eklund *et al.*, "Assessment of cerebrospinal fluid outflow resistance," *Medical and Biological Engineering and Computing*, vol. 45, no. 8, pp. 719–735, Jul 2007.

[14] F. B. Freimann *et al.*, "In vitro performance and principles of anti-siphoning devices," *Acta neurochirurgica*, vol. 156, no. 11, pp. 2191–2199, Aug 2014.

[15] P. K. Eide and W. Sorteberg, "Changes in intracranial pulse pressure amplitudes after shunt implantation and adjustment of shunt valve opening pressure in normal pressure hydrocephalus," *Acta Neurochirurgica*, vol. 150, no. 11, pp. 1141–1147, Oct 2008.

[16] G. Petrella *et al.*, "How does CSF dynamics change after shunting?" *Acta Neurologica Scandinavica*, vol. 118, no. 3, pp. 182–188, Sep 2008.

[17] S. Hakim *et al.*, "A critical analysis of valve shunts used in the treatment of hydrocephalus," *Developmental Medicine & Child Neurology*, vol. 15, no. 2, pp. 230–255, Nov 1973.

[18] M. A. Hafez and O. Kempski, "A nonlinear biomechanical model for evaluation of cerebrospinal fluid shunt systems," *Child's Nervous System*, vol. 10, no. 5, pp. 302–310, Jul 1994.

[19] M. U. Schuhmann *et al.*, "Application of clinically recorded icp patterns - an extension of conventional shunt testing," *Child's Nervous System*, vol. 16, no. 12, pp. 856–861, Dec 2000.

[20] S. Bottan *et al.*, "Phantom model of physiologic intracranial pressure and cerebrospinal fluid dynamics," *IEEE Transactions on Biomedical Engineering*, vol. 59, no. 6, pp. 1532–1538, Jun 2012.
[21] M. Schmid Daners *et al.*, "Craniospinal pressure-volume dynamics in phantom models," *IEEE Transactions on Biomedical Engineering*, vol. 59, no. 12, pp. 3482–3490, Dec 2012.
[22] I. Elixmann *et al.*, "Simulation of existing and future electromechanical shunt valves in combination with a model for brain fluid dynamics," in *Hydrocephalus*, ser. Acta Neurochirurgica Supplementum, G. A. Aygok and H. L. Rekate, Eds. Springer Vienna, 2012, vol. 113, pp. 77–81.
[23] R. Ernst, "Codesign of embedded systems: status and trends," *Design Test of Computers, IEEE*, vol. 15, no. 2, pp. 45–54, Apr 1998.
[24] R. Isermann *et al.*, "Hardware-in-the-loop simulation for the design and testing of engine-control systems," *Control Engineering Practice*, vol. 7, no. 5, pp. 643–653, May 1999.
[25] G. Ochsner *et al.*, "A novel interface for hybrid mock circulations to evaluate ventricular assist devices," *IEEE Transactions on Biomedical Engineering*, vol. 60, no. 2, pp. 507–516, Feb 2013.
[26] B. Siyahhan *et al.*, "Flow induced by ependymal cilia dominates near-wall cerebrospinal fluid dynamics in the lateral ventricles," *Journal of The Royal Society Interface*, vol. 11, no. 94, p. 20131189, Mar 2014.
[27] A. Marmarou *et al.*, "A nonlinear analysis of the cerebrospinal fluid system and intracranial pressure dynamics," *Journal of Neurosurgery*, vol. 48, no. 3, pp. 332–344, 1978.
[28] M. Czosnyka *et al.*, "Modeling of CSF dynamics: Legacy of professor anthony marmarou," *Acta Neurochirurgica Supplementum*, pp. 9–14, Nov 2012.
[29] W. Wakeland and B. Goldstein, "A review of physiological simulation models of intracranial pressure dynamics," *Computers in Biology and Medicine*, vol. 38, no. 9, pp. 1024–1041, Sep 2008.
[30] S. Stevens and W. Lakin, "Local compliance effects on the global pressure-volume relationship in models of intracranial pressure dynamics," *Mathematical and Computer Modelling of Dynamical Systems*, vol. 6, no. 4, pp. 445–465, Dec 2000.
[31] W. D. Lakin *et al.*, "A whole-body mathematical model for intracranial pressure dynamics," *Journal of Mathematical Biology*, vol. 46, no. 4, pp. 347–383, Apr 2003.
[32] S. Qvarlander *et al.*, "Postural effects on intracranial pressure: modeling and clinical evaluation," *Journal of Applied Physiology*, vol. 115, no. 10, pp. 1474–1480, Sep 2013.
[33] United States. National Aeronautics and Space Administration, *Man-systems integration standards*, ser. NASA-STD. National Aeronautics and Space Administration, 1995, no. Bd. 3.
[34] R. Cutler *et al.*, "Formation and absorption of cerebrospinal fluid in man," *Brain*, vol. 91, no. 4, pp. 707–720, 1968.
[35] M. Czosnyka *et al.*, "Cerebrospinal fluid dynamics," *Physiological Measurement*, vol. 25, no. 5, pp. R51–R76, Aug 2004.
[36] S. Bottan *et al.*, "Assessment of intracranial dynamics in hydrocephalus: effects of viscoelasticity on the outcome of infusion tests," *Journal of Neurosurgery*, vol. 119, no. 6, pp. 1511–1519, Dec 2013.
[37] W. Wakeland and B. Goldstein, "A computer model of intracranial pressure dynamics during traumatic brain injury that explicitly models fluid flows and volumes," in *Intracranial Pressure and Brain Monitoring XII*, ser. Acta Neurochirurgica Supplementum, W. Poon *et al.*, Eds. Springer Vienna, 2005, vol. 95, pp. 321–326.
[38] J. Lfgren *et al.*, "The pressure-volume curve of the cerebrospinal fluid space in dogs," *Acta Neurologica Scandinavica*, vol. 49, no. 4, pp. 557–574, 1973.
[39] H. Sullivan and J. Allison, "Physiology of cerebrospinal fluid," *Neurosurgery*, vol. 3, pp. 2125–2135, 1985.
[40] J. Drake *et al.*, "Computer modeling of siphoning for CSF shunt design evaluation," *Pediatric Neurosurgery*, vol. 21, no. 1, pp. 6–15, 1994.
[41] S. A. Stevens *et al.*, "Modeling steady-state intracranial pressures in supine, head-down tilt and microgravity conditions," *Aviation, Space, and Environmental Medicine*, vol. 76, no. 4, pp. 329–338, Apr 2005.
[42] A. Behrens *et al.*, "Are intracranial pressure wave amplitudes measurable through lumbar puncture?" *Acta Neurologica Scandinavica*, vol. 127, no. 4, pp. 233–241, Jul 2012.
[43] A. Brodbelt and M. Stoodley, "CSF pathways: a review," *British Journal of Neurosurgery*, vol. 21, no. 5, pp. 510–520, Jan 2007.
[44] B. S. Elkin *et al.*, "A detailed viscoelastic characterization of the p17 and adult rat brain," *Journal of Neurotrauma*, vol. 28, no. 11, pp. 2235–2244, Nov 2011.
[45] K. Laksari *et al.*, "Constitutive model for brain tissue under finite compression," *Journal of Biomechanics*, vol. 45, no. 4, pp. 642–646, Feb 2012.
[46] Y. Hoi *et al.*, "Characterization of volumetric flow rate waveforms at the carotid bifurcations of older adults," *Physiological Measurement*, vol. 31, no. 3, p. 291, Mar 2010.
[47] W. S. Cobb *et al.*, "Normal intraabdominal pressure in healthy adults," *Journal of Surgical Research*, vol. 129, no. 2, pp. 231–235, Dec 2005.
[48] A. Al-Hwiesh *et al.*, "Intraperitoneal pressure and intra-abdominal pressure: are they the same?" *Peritoneal Dialysis International*, vol. 31, no. 3, pp. 315–319, Feb 2011.
[49] P. Cordo *et al.*, "The sit-up: complex kinematics and muscle activity in voluntary axial movement," *Journal of Electromyography and Kinesiology*, vol. 13, no. 3, pp. 239–252, Jun 2003.
[50] I. M. Elixmann *et al.*, "Case study of relevant pressures for an implanted hydrocephalus valve in everyday life," in *Engineering in Medicine and Biology Society (EMBC), 2012 Annual International Conference of the IEEE*. IEEE, Aug 2012, pp. 1635–1638.
[51] H. Steven, "Development of a worldwide harmonised heavy-duty engine emissions test cycle," *Final Report*, Apr 2001.
[52] M. André, "The artemis European driving cycles for measuring car pollutant emissions," *Science of The Total Environment*, vol. 334, pp. 73–84, Dec 2004.
[53] D. Farahmand *et al.*, "Intracranial pressure in hydrocephalus: impact of shunt adjustments and body positions," *Journal of Neurology, Neurosurgery & Psychiatry*, vol. 86, no. 2, pp. 222–228, Jun 2014.
[54] S. Qvarlander *et al.*, "The pulsatility curve-the relationship between mean intracranial pressure and pulsation amplitude," *Physiological Measurement*, vol. 31, no. 11, p. 1517, Nov 2010.
[55] E. Foltz, "Hydrocephalus and CSF pulsatility: clinical and laboratory studies," *Hydrocephalus. Raven Press, New York*, pp. 337–362, 1984.

Manuel Gehlen is working towards his PhD at The Interface Group, Institute of Physiology, University of Zurich, Switzerland and at the Institute for Dynamic Systems and Control, ETH Zurich, Switzerland. He received his degree in Mechanical Engineering from ETH Zurich, Switzerland in 2013. His research focuses on the development of actively controlled cerebrospinal fluid shunts for the treatment of hydrocephalus.

Vartan Kurtcuoglu received his degree in mechanical engineering from ETH Zurich after completing his diploma thesis at the French National Center of Scientific Research, CNRS PROMES. The subject of his doctoral dissertation at ETH was computational modeling of CSF flow in the human ventricular system. He is currently an assistant professor of computational and experimental physiology at the University of Zurich.

Marianne Schmid Daners graduated in 2006 as a mechanical engineer at ETH Zurich, Switzerland. Under the supervision of Prof. Lino Guzzella, she received her PhD in 2012 at the Institute for Dynamic Systems and Control at ETH Zurich on the topic "Adaptive Shunts for Cerebrospinal Fluid Control". Currently, Marianne Schmid Daners leads the Biomedical Systems group of the Product Development Group Zurich and is responsible for the project coordination of the Zurich Heart. Her research interests are the modeling and control of biological systems and the development and control of biomedical devices.